Plasmon-Exciton Strong Coupling in Single-Molecule Junction Electroluminescence

Angela L. Paoletta,[†] Norah M. Hoffmann,[†] Daniel W. Cheng,[†] Emma York,[†] Ding Xu,[†] Milan Delor,[†] Timothy C. Berkelbach,[†] and Latha Venkataraman[,†,‡]

†Department of Chemistry and ‡Department of Applied Physics and Applied Mathematics, Columbia University, New York, New York 10027, United States

Abstract:

Single molecules bridging two metallic electrodes can emit light through electroluminescence when subject to a bias voltage. Typically, light emission in such devices results from transitions between molecular states although in the presence of light-matter coupling, the emission can result from a transition between hybrid light-matter states. Here, we create single metal-molecule-metal junctions and simultaneously collect conductance and electroluminescence data using a scanning tunneling microscope (STM) equipped with a custom spectrometer. Through experimental analysis and electronic structure calculations, we provide evidence for a molecule-electrode interfacial exciton coupled to the junction cavity plasmon. Importantly, we find that close to resonant transport conditions, the molecular junction functions as a single emitter that is strongly coupled to the junction cavity mode, leading to characteristic Rabi splitting of the emission spectrum and providing the first example of an electroluminescence-driven single-molecule system in the regime of strong light-matter coupling.

Recent progress in polaritonics has revealed exciting new pathways for creating novel quantum materials[1] and modifying chemical processes[2] by utilizing the strong light-matter interactions that arise when emitters are confined in optical cavities. Such strong light-matter coupling yields light-matter hybrid states, i.e. polaritons, which can significantly alter chemical landscapes and material properties without the need of driving the system externally. Strong coupling interactions between plasmonic modes and molecular emitters prove particular exciting, as these hybrid plasmon-emitter systems have novel applications in a range of technologies, including but not limited to ultrafast switching, active plasmonic devices, photovoltaics, and quantum information processing.[1] However, a main challenge to unravel many of these phenomena is the substantial disparity between possibilities in experimental and theoretical systems.[3] In experimental realizations, there is often a lack of control over the number of molecules coupling to the cavity mode, and achieving strong coupling typically relies on a collective regime involving many molecules coupled to few cavity modes. Such many-molecule systems pose significant challenges for first-principles theoretical approaches, and the mechanism by which macroscopic observables are affected by collective strong coupling remains unclear.[4] Hence, the fundamental limit of strong coupling between a plasmonic mode and a single quantum emitter could greatly contribute to closing this gap,[5,6] a triumph that has only seldomly been approached by experimental researchers working with quantum dots,[7-9] dye molecules,[10] and J-aggregates[11] as emitters. For example, Chikkaraddy et al. successfully encapsulated a few molecules via host-guest chemistry and observed molecular strong coupling within a plasmonic nanocavity through optical scattering measurements.[10]

Here, we present evidence of single-molecule strong coupling in an electroluminescent system. Using the scanning tunneling microscope break junction (STM-BJ) technique, we create

a plasmonic cavity between two Au electrodes that are bridged by a single molecule through direct donor-acceptor bonds. We apply a voltage bias across the junction, driving electron tunneling and providing a source for electroluminescence. Through simultaneous conductance and spectroscopy measurements, we observe that tunneling and light emission are maximized when resonant transport is achieved. Most interestingly, we see a split peak feature in the electroluminescence spectra of junctions biased close to the plasmon energy and resonant electronic transport conditions.[12] Through a combination of experimental and theoretical results, we attribute the electroluminescence in these junctions to emission from an interfacial exciton that is coupled to the plasmon mode of the gap, leading to light-matter hybrid states known as an exciton-polariton[10] or plexciton states.[13]

We study molecular junctions of 4,4'-bipyridine (BP), shown in Figure 1a.[14-17] Au-BP-Au junctions (abbreviated BP junctions) generally display strong negative differential resistance (NDR) at voltages between 1.8 and 2.0 V.[18] At these biases, resonant tunneling electrons will emit photons that are energetically close to the plasmonic resonance as evidenced by the spectra obtained from Au tunnel junctions.[19] Note that resonant transport/tunneling refers to an electron tunneling from the Au electrode to BP, while plasmonic resonance involves the plasmon frequency being resonant with the excitonic transition.

We measure conductance and electroluminescence simultaneously, with both time and spectral resolution. We use a custom STM-BJ setup where light emission intensity is measured by a silicon photomultiplier (SiPM, Excelitas) and reported as a time-resolved photovoltage signal acquired at 40 KHz.[18-20] The photovoltage signal indicates overall light emission intensity for the range of photon energies that the SiPM is sensitive to (400 to 1000 nm). For each junction, we also collect one spectrum using a custom spectrometer. Figure 1a shows a simplified diagram of this

experimental setup, and a more detailed diagram and description can be found in the Supplementary Information (Supplementary Figure S1).

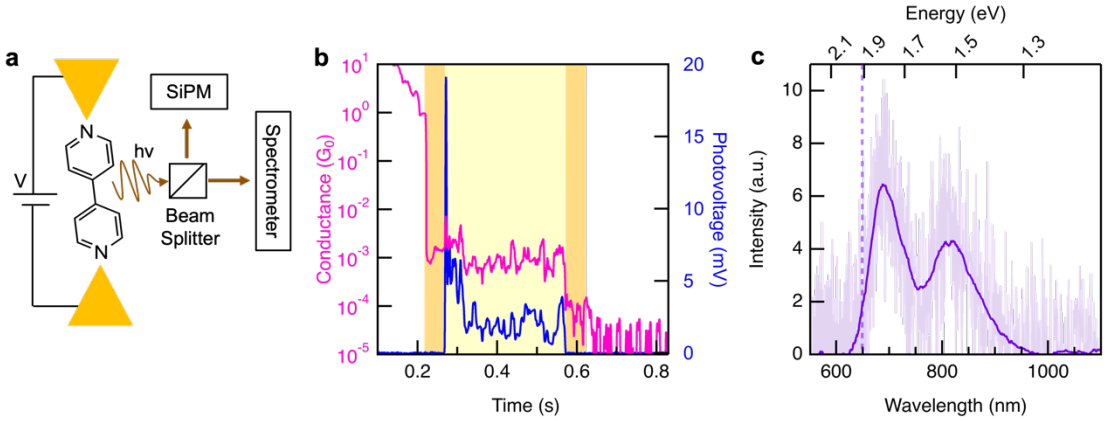

Figure 1. Experimental methods. (a) Schematic of experimental setup. A single 4,4'-bipyridine molecule bridges the gap between two Au electrodes. A bias V is applied across the junction. Light emission is measured by a silicon photomultiplier (SiPM) and a spectrometer simultaneously. (b) Time-resolved conductance and photovoltage traces for a single junction. The electrodes are held fixed in the yellow and orange highlighted region. A bias of 1.91 V is applied in the yellow highlighted region and 0.1 V is applied in the orange and white regions. (c) Spectrum of electroluminescence from the junction shown in (b) with a dotted line at 1.91 eV, the energy supplied by the bias. The dark line is a spectrum after applying a 101-point boxcar smoothing. The split peak feature indicates strong coupling.

Conductance and synchronously acquired photovoltage traces for a single BP junction subjected to a 1.91 V bias are shown in Figure 1b. We observe a plateau at 1 G_0 ($G_0 = 2e^2/h$), indicating transmission through a single-atom Au point contact. Once this contact is broken, a molecule bridges the gap between the two electrodes leading to a molecular plateau with a conductance around 10^{-3} G_0, characteristic of BP junctions.[15-17] Critically, this conductance signature ensures that we are measuring a single-molecule junction. This junction is held fixed for 300 ms (as indicated by the highlighted region in Figure 1b) and a high bias is applied to drive electroluminescence. As can be seen in the blue trace, photovoltage is elevated during this hold portion of the trace. The corresponding simultaneously-acquired electroluminescence spectrum for this junction is shown in Figure 1c. A dotted line is drawn at the energy supplied by the bias. The

clear double peak feature observed in the electroluminescence spectrum, which is due to strong coupling between the plasmon and an interfacial exciton, is discussed further below. Most of the emission is at an energy such that $h\nu < eV$ where ν is the photon frequency and V is the applied bias.

We apply this method to gather simultaneous conductance and spectral data of BP junctions at 3 different biases. We sum together the spectra from every junction that sustains a molecule to obtain an average spectrum for each bias. These average spectra are shown in Figure 2a. Analogous measurements for Au tunnel junctions are shown in Figure 2b. The molecular spectra show clear peak shift to higher energy emission as the bias is increased. The Au tunnel junction spectra however span the same energy range for all biases and show a weaker blueshift with increasing bias. Figure 2c shows peak position versus bias for both the molecular junctions and the Au tunnel junctions. BP junctions show a stronger bias dependence than Au tunnel junctions, indicating that the electroluminescence mechanism is distinct for these two types of junctions.

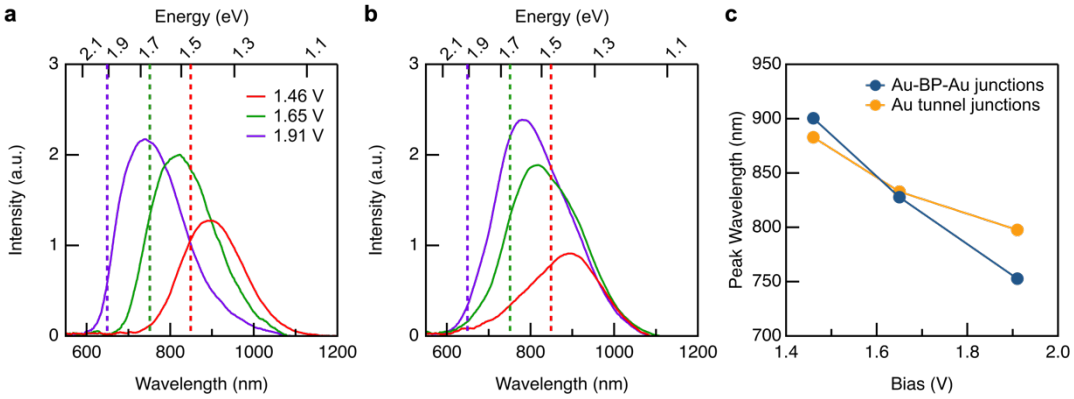

Figure 2. Averaged electroluminescence spectra of (a) Au-4,4'-bipyridine-Au junctions and (b) Au tunnel junctions at various biases. Dotted lines are drawn at 1.46 (red), 1.65 (green), and 1.91 (purple) eV. A 101-point boxcar smoothing is applied. The number of traces used to generate these spectra are as follows. BP junctions: 1.46 V: 435 traces, 1.65 V: 217 traces, 1.91 V: 240 traces. Au junctions: 1.46 V: 1930 traces,1.65 V: 1759 traces, 1.91 V: 1858 traces. (c) Plot of spectral peak wavelength as determined by Lorentzian fits versus bias.

It is likely that electron transmission through molecular orbitals affects the light emission mechanism (see Supplementary Section S3 for a discussion of transport across a molecular junction). We propose that emission through BP junctions is not entirely shot noise-driven,[18] unlike that of Au tunnel junctions, but also results from the relaxation of an interfacial exciton between BP and the electrode. We note here that emission from a pure molecular exciton is highly unlikely because the applied bias is significantly smaller than the ~5 eV optical gap of bipyridine.[19,21] Our proposed mechanism that explains these spectroscopy results is shown in Figure 3a. This mechanism features a metal-molecule interfacial exciton, which has previously been proposed for metal-semiconductor systems,[22,23] and is also corroborated by time-dependent density-functional theory (TD-DFT) calculations discussed further below. Here an electron is injected into the dominant electron transport channel,[16,17] the lowest unoccupied molecular orbital (LUMO) of BP, which is broadened by interactions with Au. The electron then recombines with a hole in the electrode to emit a photon with an energy that is less than that provided by the bias.

We now turn to the double peak feature seen in Figure 1c, which we attribute to light emission from the interfacial exciton that is strongly coupled to the plasmon. We observe a split peak feature in the spectra of a significant fraction of the BP junctions when the applied bias is 1.91 V or 1.65 V, but not 1.46 V. The effect of plasmon-exciton coupling is expected to be strongest when the energy of the plasmon matches that of the exciton, explaining why this split peak feature occurs most frequently at the biases closest to the peak of the plasmon resonance (estimated to be around 1.5 – 1.8 eV from the Au tunnel junction spectra data), and at the biases for which the lifetime of the electron on the molecule is longest (i.e. close to when resonant transport is achieved, around 1.8 - 2.0 V).[24,25]

To test our hypothesis, we consider our experimental system as two coupled oscillators illustrated in Figure 3b and described by the Hamiltonian

$$H = \begin{bmatrix} \omega_0 - i\gamma_0/2 & g \\ g & \omega_p - i\gamma_p/2 \end{bmatrix},$$

where ω_0 and ω_p are the energies of the exciton and plasmon resonances, γ_0^{-1} and γ_p^{-1} are the lifetimes of the exciton and plasmon respectively ($\gamma = 0$ indicates an infinite lifetime), and g is the coupling strength (note that our convention for the definition of g is a factor of two smaller than that of Chikkaraddy, R. *et al.*[10] and Park *et al.*[26]). With this Hamiltonian, we can obtain the eigenvalues of the hybridized states as:

$$\omega_{\pm} = \frac{1}{2}(\omega_p + \omega_0) \pm \frac{1}{2}\sqrt{4g^2 + \delta^2 - \frac{1}{4}(\gamma_0 - \gamma_p)^2} \quad (1)$$

Here, $\delta = \omega_p - \omega_0$ is the detuning energy. To determine the coupling, oscillator frequencies, and lifetimes, we model the emission for this two-oscillator system as detailed in Supplementary Section 4 and fit the experimental spectra with Equation S1. For the data in Figure 1c (see Supplementary Figure S4a) we obtain $g = 0.16$ eV, $\gamma_0 = 0.23$ eV, and $\gamma_p = 0.10$ eV. We see that $2g > \gamma_0, \gamma_p$ which confirms strong coupling between the cavity plasmon and interfacial exciton to form upper and lower polaritons (or plexcitons).[27] Furthermore, since both $\gamma_0, \gamma_p > 0$, we are also not in a regime where the lifetime of one of the oscillators is very large which could lead to a Fano resonance (see Supplementary Figure S4b).[28,29]

Next, we repeat the experiment without the beam splitter, directing all collected light towards the spectrometer to increase our signal to noise ratio. Focusing on the 1.91 V bias (analysis of the data collected at 1.65 V bias is in Supplementary Section S5), we observe a double peak feature in the experimental spectra of 160 BP junctions (~ 25% of the molecular junctions that

produce a spectrum with sufficiently high intensity necessary for the analysis). We fit these spectra with Equation S1 constraining ω_0, the exciton frequency, to 1.62 eV. This frequency is determined from spectra of molecular junctions that show a clear single peak (25% of spectra with sufficiently high intensity necessary for the analysis, see Supplementary Figure S4c). We assume that ω_0 remains the same across all junctions, as is also done in other works.[10,11,26,30,31] The fitting gives γ_0, γ_p, and g for each individual junction. We find that 71 of these junctions fall into the strong coupling regime, with $2g > \gamma_0, \gamma_p$.[27] We show these spectra in Figure 3c and 12 of these spectra, along with their fits, in Supplementary Figure S4. 85 junctions have $2g < \gamma_0, \gamma_p$. These are classified as weak coupling (see Supplementary Figure S5 for comparison). The remaining junction spectra could not be fit successfully with our automated fitting procedure.

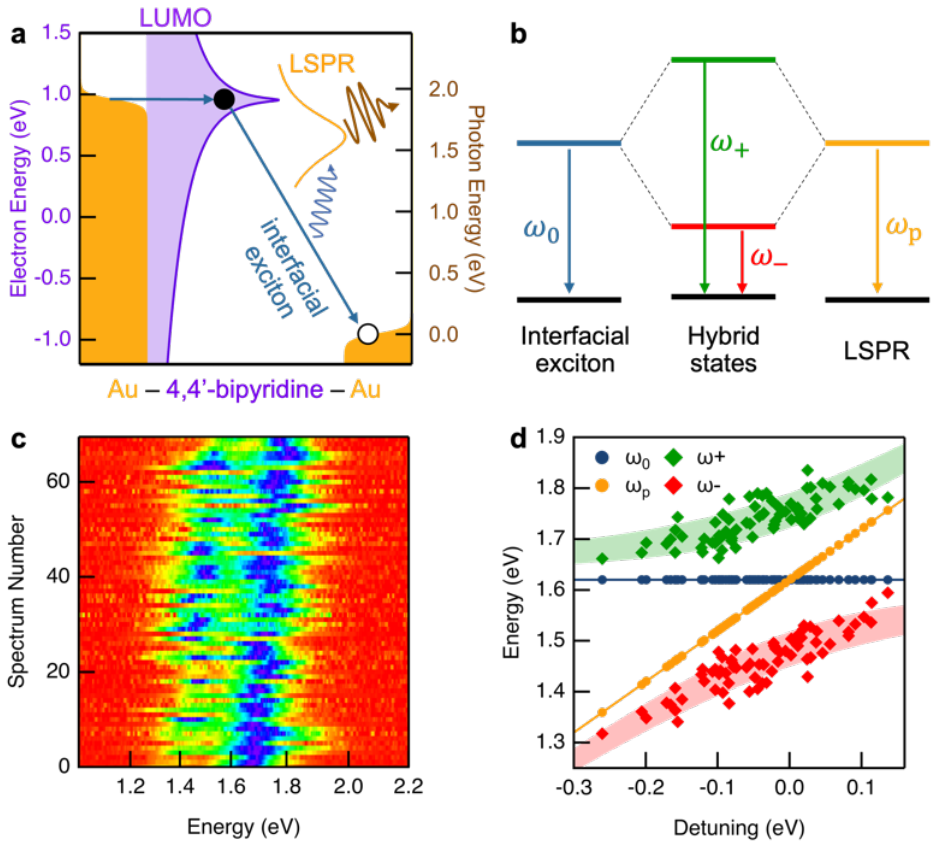

Figure 3. Light-matter coupling. (a) Proposed light emission mechanism in which an electron is injected into the LUMO from the substrate, forming an interfacial exciton with a hole in the electrode. Electron-hole pair recombination can emit a photon directly or excite the localized

surface plasmon resonance (LSPR). Or, emission can proceed through hybrid plasmon-exciton states. Electron energy is relative to the Fermi energy. (b) Schematic of light-matter coupling between an interfacial excitation and the LSPR. (c) Two-dimensional spectra of junctions that display strong coupling plotted in order of detuning. (d) Plot of energy versus detuning for the exciton (ω_0), plasmon (ω_p), and upper and lower polariton (ω_+, ω_-) determined from single-molecule junction spectra, showing an avoided crossing. The shaded regions show calculated values using the average coupling obtained from all fits, g = 0.14 $\pm$ 0.03 eV. The diamond symbols are data points extracted from the experimental electroluminescence spectra.

For the junctions in the strong coupling regime, we plot ω_0, ω_p, ω_+ and ω_- versus δ, the detuning (Figure 3d). We first note that ω_p varies from junction to junction, as has been found before because the tip shape affects the plasmon mode.[32] The range of ω_p found here fits well within the average spectrum obtained for Au tunnel junctions shown in Figure 2b. We observe an avoided crossing. The average g from the 71 spectra that fall into the strong-coupling regime is 0.14 eV. Using this average g and a standard deviation of 0.03 eV, we obtained the shaded regions shown in Figure 3d.

To elucidate and validate the interfacial exciton and strong light-matter coupling, we performed TD-DFT calculations using the ORCA[33] quantum chemistry package with the B3LYP functional[34,35] and the def2-TZVP basis set.[36,37] The BP geometries were fully optimized using the same functional and basis set. We employed two four-layered fcc-Au pyramids simulating the STM electrodes, with BP placed in between. We calculated the absorption spectra, shown in Figure 4a, in three scenarios: 1) BP only (in green), 2) the Au electrodes only (in orange), 3) BP trapped between the Au electrodes (in blue).

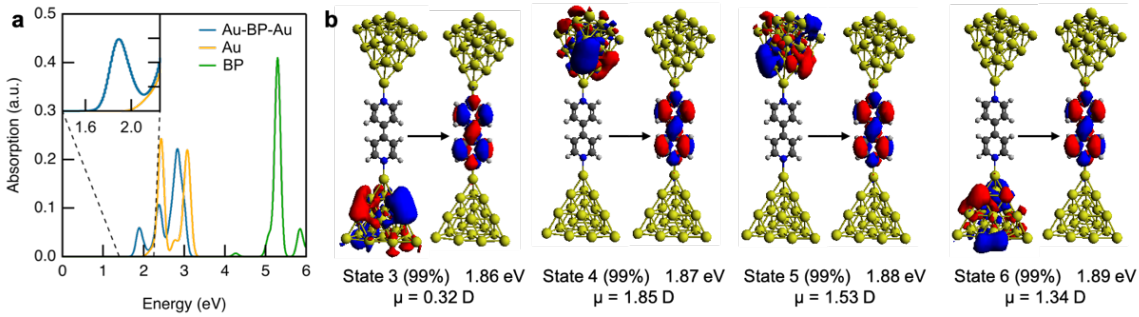

Figure 4. TD-DFT results. (a) Calculated absorption spectra with the region below 2 eV expanded in the inset where a clear peak is visible at 1.9 eV. (b) Calculated natural transition orbitals (NTOs) for the excited states of the Au-BP-Au system. For each state, the hole is shown on the left and the electron on the right, along with the excitation energy and transition dipole moment. The percentage shows the contribution of the pair of orbitals to the overall transition.

We confirm that the optical transition of the pure BP occurs around 5 eV (Figure 4a, green trace), which surpasses the plasmon mode, and therefore cannot be excited with biases used here or effectively couple to the plasmon mode. However, placing BP between the two Au electrodes results in absorption at low energies (< 2 eV, see inset of Figure 4a), supporting the hypothesis of an interfacial exciton between Au and BP with energies near the plasmon frequency. These lower energy transitions are not seen in the calculated spectrum of the isolated Au electrodes (orange trace in Figure 4a), confirming that they are unique to the metal-molecule-metal junction.

To characterize the interfacial exciton, we calculated the natural transition orbitals (NTOs) for the low-energy excited states (Figure 4b). The four lowest-energy states are all interfacial excitons, with the electron on the molecule (essentially the molecular LUMO) and the hole delocalized over the Au electrode. This supports the hypothesis that, after resonant transport excites the system (i.e. creates the interfacial exciton), electrons in the molecular LUMO combine with holes above the highest occupied orbital of the electrode.

Finally, we use our TD-DFT calculations to estimate the coupling strength for a single molecule,[10]

$$g = \mu_{eff}\sqrt{\frac{\pi\hbar c}{\lambda\varepsilon\varepsilon_0 V}} \qquad (2)$$

where λ is the wavelength, ε is the absolute permittivity, ε_0 is the permittivity in free space, and V is the cavity volume. We use λ = 663 nm (or 1.87 eV), $\varepsilon = \varepsilon_0 = 1$, and $V = 1$ nm^3. For our model of the junction, we find that the four lowest-energy transitions are all approximately degenerate with similar transition dipole moments (Figure 4b). Thus, we calculate an effective dipole moment of $\mu_{eff} = \sqrt{N}\mu_m = 3.6\ D$, where $N = 4$ is the number of degenerate transitions and μ_m is the transition dipole moment of a single transition. This yields a coupling strength of g = 0.09 eV, in good agreement with the experimental g = 0.14 eV. The details of this calculation will change depending on computational choices such as the functional or the size and geometry of the Au electrodes, nonetheless, this calculation confirms that a coupling strength of g = 0.14 eV for an interfacial exciton is physically realistic (see Supplementary Section S6 for additional discussions, including calculated coupling using different cavity volumes). Finally, we highlight that the experimental coupling strength of 0.14 eV aligns closely with that previously reported by Baumberg and coworkers in a comparable plasmonic system.[10] In their study, they note an average of 2.5 molecules in the cavity with a coupling strength of 0.15 eV (using our definition of g).

In conclusion, we show that the emission from BP tunnel junctions is impacted by transmission through the LUMO of BP. We achieved strong light-matter coupling by coupling an interfacial exciton to the gap plasmon mode created between the STM tip and substrate. We confirm that we are in the single-molecule regime through our simultaneous conductance measurements that accompany the spectrum gathered for each junction. The strong coupling mechanism requires that the interfacial exciton is resonant with the junction plasmon, and thus could be observed for other molecular junctions that have a molecular resonance between 1.8 and 2.0 eV when using Au electrodes. This plexciton formation is likely the first demonstration of

strong light-matter coupling in electroluminescence at the single-molecule level and under ambient conditions, opening up new avenues for highly controllable experiments in polaritonic chemistry.

Acknowledgements

A.L.P was supported by the National Defense Science and Engineering Graduate Fellowship. N.M.H. was supported by a fellowship of the German National Academy of Science Leopoldina and by the U.S. Air Force Office of Scientific Research, under Grant No. FA9550-21-1-0400. This research was supported in part by the National Science Foundation under grant CHE-2023568. M.D. acknowledges support from the National Science Foundation under grant CHE-2203844 and from the Arnold and Mabel Beckman Foundation through a Beckman Young Investigator award.

References

1. Ashida, Y. et al. Quantum Electrodynamic Control of Matter: Cavity-Enhanced Ferroelectric Phase Transition. *Phys.Rev. X* **10** (2020).
2. Thomas, A. et al. Tilting a ground-state reactivity landscape by vibrational strong coupling. *Science* **363**, 615-619 (2019).
3. Sanchez-Barquilla, M., Fernandez-Dominguez, A. I., Feist, J. & Garcia-Vidal, F. J. A Theoretical Perspective on Molecular Polaritonics. *ACS Photonics* **9**, 1830-1841 (2022).
4. Du, M., Poh, Y. R. & Yuen-Zhou, J. Vibropolaritonic Reaction Rates in the Collective Strong Coupling Regime: Pollak–Grabert–Hänggi Theory. *The Journal of Physical Chemistry C* **127**, 5230-5237 (2023).
5. Qin, J. et al. Revealing Strong Plasmon-Exciton Coupling between Nanogap Resonators and Two-Dimensional Semiconductors at Ambient Conditions. *Phys Rev Lett* **124**, 063902 (2020).

6. Li, W. et al. Highly Efficient Single-Exciton Strong Coupling with Plasmons by Lowering Critical Interaction Strength at an Exceptional Point. *Phys Rev Lett* **130**, 143601 (2023).
7. Santhosh, K., Bitton, O., Chuntonov, L. & Haran, G. Vacuum Rabi splitting in a plasmonic cavity at the single quantum emitter limit. *Nat. Commun.* **7**, ncomms11823 (2016).
8. Groß, H., Hamm, J. M., Tufarelli, T., Hess, O. & Hecht, B. Near-field strong coupling of single quantum dots. *Science Advances* **4**, 1-8 (2018).
9. Li, J. Y. et al. Room-Temperature Strong Coupling Between a Single Quantum Dot and a Single Plasmonic Nanoparticle. *Nano Lett* **22**, 4686-4693 (2022).
10. Chikkaraddy, R. et al. Single-molecule strong coupling at room temperature in plasmonic nanocavities. *Nature* **535**, 127-30 (2016).
11. Liu, R. et al. Strong Light-Matter Interactions in Single Open Plasmonic Nanocavities at the Quantum Optics Limit. *Phys. Rev. Lett.* **118**, 237401 (2017).
12. Zhu, Y. et al. Electroluminescence as a Probe of Strong Exciton–Plasmon Coupling in Few-Layer WSe2. *Nano Lett.* **24**, 525-532 (2024).
13. Zhu, Y. et al. Electroluminescence as a Probe of Strong Exciton-Plasmon Coupling in Few-Layer WSe(2). *Nano Lett* **24**, 525-532 (2024).
14. Xu, B. & Tao, N. J. Measurement of Single-Molecule Resistance by Repeated Formation of Molecular Junctions. *Science* **301**, 1221-1223 (2003).
15. Quek, S. Y. et al. Mechanically controlled binary conductance switching of a single-molecule junction. *Nat. Nanotechnol.* **4**, 230-4 (2009).

16. Kim, T. et al. Determination of energy level alignment and coupling strength in 4,4'-bipyridine single-molecule junctions. *Nano Lett.* **14**, 794-8 (2014).

17. Fung, E. D., Adak, O., Lovat, G., Scarabelli, D. & Venkataraman, L. Too Hot for Photon-Assisted Transport: Hot-Electrons Dominate Conductance Enhancement in Illuminated Single-Molecule Junctions. *Nano Lett.* **17**, 1255-1261 (2017).

18. Paoletta, A. L. & Venkataraman, L. Determining Transmission Characteristics from Shot-Noise-Driven Electroluminescence in Single-Molecule Junctions. *Nano Lett.* **24**, 1931-1935 (2024).

19. Paoletta, A. L., Fung, E. D. & Venkataraman, L. Gap Size-Dependent Plasmonic Enhancement in Electroluminescent Tunnel Junctions. *ACS Photonics* **9**, 688-693 (2022).

20. Fung, E. D. & Venkataraman, L. Too Cool for Blackbody Radiation: Overbias Photon Emission in Ambient STM Due to Multielectron Processes. *Nano Lett.* **20**, 8912-8918 (2020).

21. Coleman, B. D. & Fuoss, R. M. Quaternization Kinetics. I. Some Pyridine Derivatives in Tetramethylene Sulfone. *J. Am. Chem. Soc.* **77**, 5 (1955).

22. Wu, K., Chen, J., McBride, J. R. & Lian, T. Efficient hot-electron transfer by a plasmon-induced interfacial charge-transfer transition. *Science* **349**, 4 (2015).

23. Dutton, G., Quinn, D. P., Lindstrom, C. D. & Zhu, X. Y. Exciton dynamics at molecule-metal interfaces:C60⁄Au(111). *Phys.Rev. B* **72** (2005).

24. Adak, O. et al. Ultrafast Bidirectional Charge Transport and Electron Decoherence at Molecule/Surface Interfaces: A Comparison of Gold, Graphene, and Graphene Nanoribbon Surfaces. *Nano Lett.* **15**, 8316-21 (2015).

25. Cvetko, D. et al. Ultrafast electron injection into photo-excited organic molecules. *Phys. Chem. Chem. Phys.* **18**, 22140-5 (2016).

26. Park, K.-D. et al. Tip-enhanced strong coupling spectroscopy, imaging, and control of a single quantum emitter. *Sci. Adv.* **5**, 1-7 (2019).

27. Thomas, P. A., Tan, W. J., Fernandez, H. A. & Barnes, W. L. A New Signature for Strong Light–Matter Coupling Using Spectroscopic Ellipsometry. *Nano Lett.* **20**, 6412-6419 (2020).

28. Nian, L.-L., Wang, Y. & Lü, J.-T. On the Fano Line Shape of Single Molecule Electroluminescence Induced by a Scanning Tunneling Microscope. *Nano Lett.* **18**, 6826-6831 (2018).

29. Limonov, M. F., Rybin, M. V., Poddubny, A. N. & Kivshar, Y. S. Fano resonances in photonics. *Nat. Phot.* **11**, 543-554 (2017).

30. Nian, L.-L. & Lü, J.-T. Mechanism of Bimodal Light Emission in a Molecule-Mediated Scanning Tunneling Microscopy Junction. *J. Phys. Chem. C* **123**, 18508-18515 (2019).

31. Zhang, Y. et al. Sub-nanometre control of the coherent interaction between a single molecule and a plasmonic nanocavity. *Nat. Commun.* **8**, 15225 (2017).

32. Aizpurua, J., Apell, S. P. & Berndt, R. Role of tip shape in light emission from the scanning tunneling microscope. *Physical Review B* **62**, 2065-2073 (2000).

33. Neese, F. Software update: the ORCA program system, version 4.0. *WIREs Comput. Mol. Sci.* **8** (2017).

34. Becke, A. D. Density-functional exchange-energy approximation with correct asymptotic behavior. *Phys. Rev. A Gen. Phys.* **38**, 3098-3100 (1988).

35. Becke, A. D. A new mixing of Hartree–Fock and local density-functional theories. *J. Chem. Phys.* **98**, 1372-1377 (1993).

36. Schäfer, A., Huber, C. & Ahlrichs, R. Fully optimized contracted Gaussian basis sets of triple zeta valence quality for atoms Li to Kr. *J. Chem. Phys.* **100**, 5829-5835 (1994).

37. Weigend, F. & Ahlrichs, R. Balanced basis sets of split valence, triple zeta valence and quadruple zeta valence quality for H to Rn: Design and assessment of accuracy. *Phys. Chem. Chem. Phys.* **7**, 3297-305 (2005).

For Table of Contents Only: